Threshold Hydrophobicity for Inhibition of Salt Scale Formation on SAM-Modified Titania Nanotube Arrays

Lian C. T. Shoute[1†], Weidi Hua[1†], Ryan Kisslinger[1], Ujwal K. Thakur,[1] Sheng Zeng,[1] Ankur Goswami,[1] Pawan Kumar,[1] Piyush Kar[1*] and Karthik Shankar[1, 2]*

[1]Department of Electrical and Computer Engineering, University of Alberta, 9211 - 116 St, Edmonton, Alberta, Canada T6G 1H9
[2]NRC National Institute for Nanotechnology, 11421 Saskatchewan Drive NW, Edmonton, AB T6G 2M9, Canada

*Email: Karthik Shankar (kshankar@ualberta.ca), Piyush Kar (pkar1@ualberta.ca)
†Authors who contributed equally

Abstract

Fouling of solid surfaces is a ubiquitous problem in industrial processes. As unwanted material accumulates on components, their function is impaired and costly repairs are required. Most fouling occurs from impurities present in water that are deposited when the water contacts a solid surface. It follows that if the adhesive forces at the water-solid interface are minimized, less fouling will result. In this study, we present a novel method to minimize fouling by fabricating a hydrophobic surface based upon self-assembled monolayer (SAM)-modified titanium dioxide nanotube arrays (TNTAs). We demonstrate a direct correlation between hydrophobicity and the formation of scale from dissolved salts by comparison of the surface's static contact angle and degree of precipitation deposition. Furthermore, by tailoring the surface hydrophobicity through employment of a wide variety of SAMs with different alkyl chain lengths, we determine the threshold level of hydrophobicity that inhibits fouling in the SAM-TNTA system; surfaces with a static contact angle greater than 144° display vastly increased fouling resistance. The surface morphology, surface composition, and stability of the alkyl phosphonic acid- and perfluoroalkyl phosphonic acid-SAM-TNTAs were characterized using scanning electron microscopy (SEM),

energy-dispersive x-ray spectroscopy (EDX), and diffuse reflectance infrared Fourier transform spectroscopy (DRIFTS).

1. Introduction

Fouling is a term used to describe the accumulation of any unwanted materials on a solid surface [1-5]. The materials which cause fouling can be organic/inorganic compounds, particles, bacteria and other living organisms. The nature of the deposit formed depends on the mechanism of its formation e.g. precipitation, sedimentation, crystallization/scaling, chemical metathesis, corrosion, and biofilm formation [1-7]. Fouling of the surface of any component of a system has an adverse effect on its function e.g. fouling of a heat exchanger or a boiler is known to drastically reduce the thermal efficiency, fouling of a pipeline reduces the fluid flow, fouling on the ship hulls creates additional drag *etc* [1-5, 8-11]. These problems need regular maintenance otherwise they are often the cause of serious degradation problems that may limit the life of components or entire industrial plants with huge economic impact. It is estimated that the economic cost due to the fouling of heat exchangers alone in the industrialized nations amount to about 0.25 % of the Gross Domestic Product (GDP) [3, 11, 12].

Fouling is an interfacial phenomenon and occurs at the interface between a solid surface and water which acts as a conduit to transport materials to the surface [12, 13]. Contact between water and solid surface which results in wetting is enabled by interactions between the molecules constituting the two materials [14-16]. The degree of wetting is determined by the balance between adhesive (interaction between different types of molecules) and cohesive forces (interaction between the same type of molecules). A manifestation of cohesive force is surface tension which is responsible for the shape of the liquid droplet.

An experimental parameter normally used to characterize the wettability of a solid surface by water is the contact angle [17-23]. The static contact angle (SCA) is the angle between the tangents to the water-air interface and to the solid surface at the line of contact between the three phases. For an ideal smooth, planar and chemically homogeneous surface, Young's equation [24] provides a relationship between the contact angle θ, the surface tension of the water σ_w, the interfacial tension σ_{sw} between water and solid and the surface free energy σ_s of the solid as

$$\sigma_s = \sigma_{sw} + \sigma_w \cos\theta \qquad (1)$$

However, most solids have rough surfaces. To account for wetting on rough and chemically homogeneous surfaces, Wenzel [25] derived the relation:
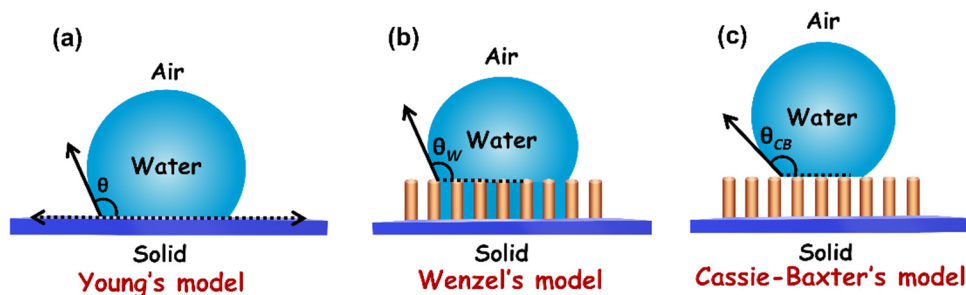
$$\cos\theta_w = r\cos\theta \qquad (2)$$

where, θ_W and θ are the rough (Wenzel) and the ideal (smooth planar) surface contact angles respectively, and r is the roughness ratio, defined as the ratio of the true area of the solid surface to the smooth planar area. In the Wenzel model, the water uniformly wets the entire surface and described the case of surfaces with a high surface energy. A model which accounts for surface heterogeneity and thus heterogenous wetting is given by Cassie and Baxter [26] equation:

$$\cos\theta_{CB} = f_s \cos\theta_c + f_v \cos\theta_v \qquad (3)$$

where θ_c is the intrinsic contact angle on the original smooth surface and f_s and f_v are the area fractions of the solid and vapor on the surface, respectively. When air pockets are trapped in the grooves of a rough surface, since the contact angle of water suspended in air is 180°, the equation simplifies to:

$$\cos\theta_{CB} = f_s (\cos\theta_c + 1) - 1 \qquad (4)$$

Schematic illustration of the wetting models represented by equation 1-4 and the experimentally determined static contact angles (SCA) characterizing the wettability of the surfaces are shown is scheme 1.

Scheme 1. Models used to describe wetting of solid surfaces by a liquid (water): (a) Young's, (b) Wenzel's, and (c) Cassie-Baxter's model and their mathematical representations as presented in equation 1-4. The parameters, θ, θ_W, and θ_{CB} are the experimentally determined static contact angles characterizing the wettability of the surfaces.

The contact angle of a water droplet on solid surfaces can be varied by functionalizing the surface with different self-assembled monolayers (SAMs). Proximal headgroups such as carboxylic acid, phosphonic acid, hydroxamic acid, trichlorosilane and thiols are used to tether SAM-forming molecules to disparate surfaces such as metal oxides, glasses, silicon, base metals and noble metals [27-33]. SAMs with distal hydroxyl, carboxylic acid, and sulfonic acid groups can be used to impart hydrophilicity to the surface, while on the other hand, surface hydrophobicity can be imparted using SAMs with distal methyl and perfluoromethyl groups [13, 17, 20, 34-37]. Surfaces with contact angle $< 90^\circ$ are considered to be hydrophilic while hydrophobic surfaces have contact angle $> 90^\circ$. The maximum hydrophobicity which can be attained by chemical modification of planar surfaces typically possessed contact angles of *ca.* 120° and the achievement of solid surfaces with contact angles $> 120^\circ$ requires texturing the surface to generate micro-scale

roughness [17, 20]. In recent years, the fabrication of micro- and nano-structured materials with superhydrophobic surfaces having contact angles > 150° has attracted enormous attention due to the wide-ranging commercial applications of surfaces with anti-fouling, anti-icing, anti-fogging, anti-biofouling, self-cleaning, drag reduction, corrosion resistance, and stain-resistant properties [38-47].

Recently, Jiang et al. studied the effect of superhydrophobicity on the scaling of $CaCO_3$ on the surface of CuO nanowires [48]. They reported that the amount of $CaCO_3$ deposited on CuO nanowires (SCA = 4.5°) reduced from 0.63 mg/cm^2 on the as-prepared CuO nanowires to 0.16 mg/cm^2 when the CuO nanowires were made superhydrophobic (SCA = 154°) with a SAM of *1H,1H,2H,2H*-perfluorodecyltriethoxysilane. Tesler et al. [49] reported durable omniphobic anti-fouling steel surfaces by electrodeposition of nanoporous tungsten oxide film on steel surfaces. The intrinsically superhydrophilic as-deposited tungsten oxide surface on steel was rendered superhydrophobic by surface functionalization with a perfluorinated alkylphosphonate monolayer followed by treatment with a fluorinated lubricant to obtain the omniphobic material. The omniphobic material was reported to inhibit the attachment of aquatic microorganisms preventing bio-corrosion and fouling of steels. Li at al. [50] reported fabrication of a self-cleaning, anticorrosion, anti-scaling, superhydrophobic hierarchical nanostructured Cu/Zn oxide on a steel pipe obtained by electrodeposition followed by oxidation in alkaline solution and functionalization with pentadecafluorooctanoic acid. A dramatic improvement of anticorrosive properties was reported by Yao et al. [51] for Cu foil with a superhydrophobic surface. The superhydrophobic surface was prepared by surface modification of alkaline solution etched nanostructured Cu oxide layer with trichloro(*1H,1H,2H,2H*-perfluorooctyl) silane to obtain a contact angle of 169°. The corrosion rate of the superhydrophobic copper foil showed a 100-fold decrease compared to the

pristine Cu and trichlorosilane modified Cu foils. With regards to biofouling, Friedrich et al. demonstrated increased density of osteoblast cells and strong biophysical cell-substrate interactions on superhydrophilic bare TiO_2 nanotubes [52], but also showed that deposition of AgO nanoparticles on TiO_2 nanotubes imparted cytotoxic and anti-microbial properties to them [53].

Despite the enormous interest worldwide in SAM functionalized and superhydrophobic materials due to their potential applications in anti-fouling and corrosion prevention, there has been no attempt to the best of our knowledge, to explore how varying the degree of surface wettability affects the fouling of the material. The as-anodized titania nanotubes are very hydrophilic [54] but can be rendered hydrophobic through suitable surface functionalization. We have previously reported on superhydrophobic films, membranes and colloidal films based on alkylphosphonate-functionalized titania nanowires and nanotubes that exhibited superior surface passivation, high impact resistance, reduced non-specific binding, and enhanced corrosion resistance [55-60]. In particular, we recently demonstrated that TNTAs functionalized with alkylphosphonate and perfluoroalkylphosphonate SAMs exhibit enhanced resistance to corrosion in salt water solutions as shown by Tafel plots manifesting a significantly higher polarization resistance in comparison to the bare TNTAs [61]. The salt water corrosion resistance of SAM-coated TNTAs was shown to be superior to that of the commercial RUST-OLEUM@TNTA anti-corrosion coating [61]. In this paper, we report on the effect of varying the wettability on the precipitation deposition of NaCl and $MgCl_2$ salts from aqueous solutions on the surface of SAM modified TNTAs on Ti foil substrates. SAMs of different alkyl chain lengths were used to tune the contact angle of the surface from 23° (hydrophilic) to 154° (superhydrophobic). The contact angle increases with an increase in alkyl chain length. The precipitation deposition of the salts on the surface as a function of the contact angle yields the threshold hydrophobicity with a contact

angle of approximately 144º to inhibit fouling. The hydrophobic and superhydrophobic TNTAs on Ti foil were stable even after many heating and cooling cycles indicating the robustness of the system.

2. Experimental

2.1 Materials

Methanol (99.8%), ethylene glycol (99.9%) and ammonium fluoride (98.3%) were obtained from Fisher Scientific. Deionized (DI) water used for contact angle measurements was obtained from ELGA system (PURELAB Ultra, ELGA). Titanium foil 99.7% and *n*-octadecyl phosphonic acid 97% were from Alfa Aesar. Glycerol 98%, *n*-decylphosphonic acid (DPA) 97 %, *n*-hexylphosphonic acid (HPA) 95%, *n*-butylphosphonic acid (BPA) and *tert*-butylphosphonic acid (TBPA) 98%, were purchased from Aldrich and used as received. *1H,1H',2H,2H'-*perfluoroodecylphosphonic acid (PFDPA) was purchased from Aculon Inc.

2.2 Sample Preparation

Ti foils for anodization were cleaned by successive sonication in soap water, acetone, 2-propanol, and methanol for 5-10 minutes each and dried in a stream of nitrogen. Titania nanotube arrays (TNTAs) were prepared by anodization of 1 cm x 4 cm Ti foil in 0.3 wt % NH_4F **and 4% DI** in ethylene glycol at 60 V for 2 hours. The samples after anodization were washed with deionized water followed by methanol and dried in a stream of nitrogen. Functionalization of TNTAs was achieved by immersing TNTA into 1-5 mM alkylphosphonic acid or PFDPA in methanol and allowing the system to equilibrate overnight (18-20 hours). The SAM modified TNTAs (SAM-TNTAs) were washed with methanol and dried in a stream of nitrogen.

2.3 Characterization

The morphologies of the nanotubes including their length, diameter, wall thickness, and separation were investigated using a scanning electron microscope (SEM, ZEISS) as well as a field-emission scanning electron microscope (FESEM, JEOL 6301F). Tapping mode Atomic force microscopy (AFM) from Bruker dimension was used to determine the surface roughness. Energy-dispersive X-ray spectroscopy (EDX) was used to characterize the surface chemical composition of the samples using an accelerating voltage of 10 kV. Kruss DSA 100 (Kruss GmbH, Hamburg, Germany) with the sessile drop technique was used to measure the contact angles. FTIR was performed using an IS5 FTIR spectrometer (Thermo Nicolet Nexus 670) equipped with a DRIFTS accessory. DRIFTS spectra of the samples were measured by mixing FTIR grade KBr with scraped-off functionalized TiO_2 nanotube powder in a DRIFTS sample cell. DRIFTS was used to verify the surface functionalization of SAM-TNTAs and monitor any changes in the SAM layer of the SAM-TNTA sample due to the heating-evaporation-deposition cycles.

3. Results and discussion

The experimental approach to prepare the nanostructured surface and tune the wettability of the surface from hydrophilic to superhydrophobic is presented in Figure 1. In summary, TNTAs are formed on titanium foil by electrochemical anodization and are then functionalized with alkyl or fluoroalkyl phosphonic acids of varying chain lengths. The surface energy of the SAM-TNTA varies with alkyl chain lengths, thereby tuning the wettability and thus the anti-fouling properties of the surface. Verification of SAM formation and stability was accomplished through DRIFTS; in this technique, the presence of certain bands in the infrared spectrum is used to verify the formation of a monolayer of molecules bound to high surface area samples such as TNTAs. Fig. 2 presents the DRIFTS spectra of SAM-TNTA samples after functionalization of TNTAs with the

alkyl- and fluoroalkyl phosphonic acids listed in Table 1. The spectra show the characteristic phosphonate and alkane bands in the 1100-1200 cm^{-1} and 1300-1500 cm^{-1} respectively. For PFDPA-TNTA the characteristic C-F stretch 1100-1300 cm^{-1} region is the strongest band in the spectrum and a weak band exists in the 2800-3000 cm^{-1} region. As the number of carbon atoms in the alky chain of the alkanephosphonic acid increased, the peaks corresponding to the symmetric- and antisymmetric $-CH_2$ stretches (Figure 2) were found to noticeably narrow in width (sharpen) and shift to lower wave numbers, indicative of decreasing disorder in the SAM. These spectra are in agreement with prior reports, and show that the functionalization protocol used in the surface modification of TNTA led to the formation of the desired alkyl or fluorinated alkyl phosphonate monolayers on the surfaces of TNTAs [57-60].
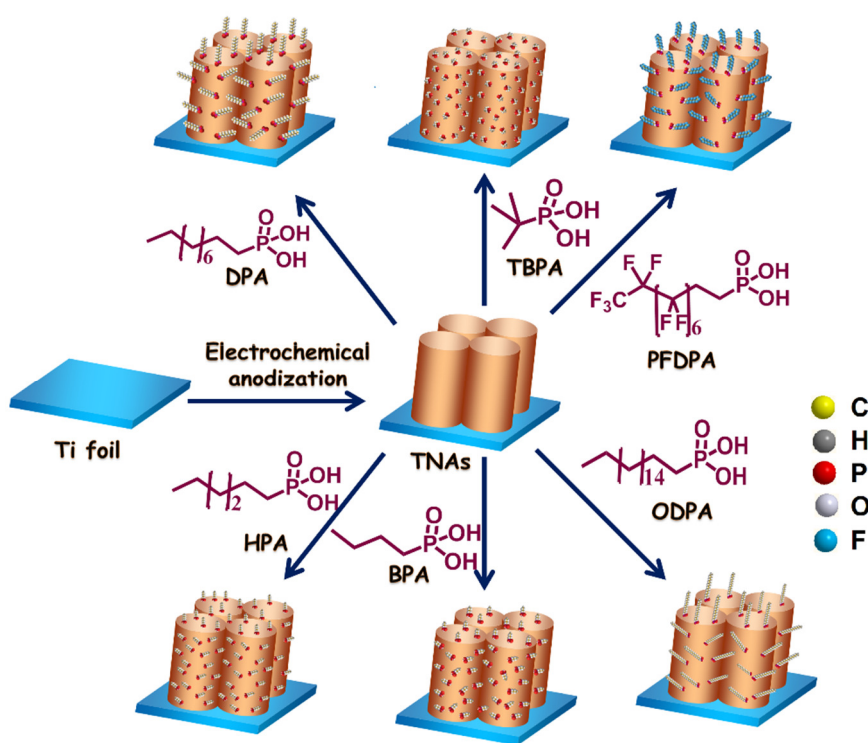

Figure 1. Schematic of the process flow used to produce the SAM-TNTAs investigated in this study, involving electrochemical anodization of Ti foil to form TNTAs followed by surface functionalization to form self-assembled monolayer on the TNTA to tune the wettability of the surface.
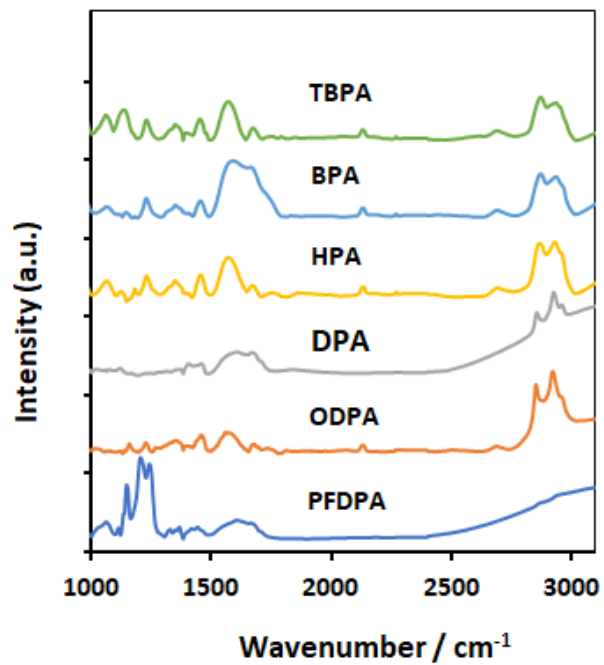
Figure 2. DRIFTS spectra of SAM-TNTA samples recorded after functionalization with alkyl or fluorinated alkyl phosphonic acids. These spectra were recorded before exposing them to the saline solution and heating-evaporation deposition fouling cycles.
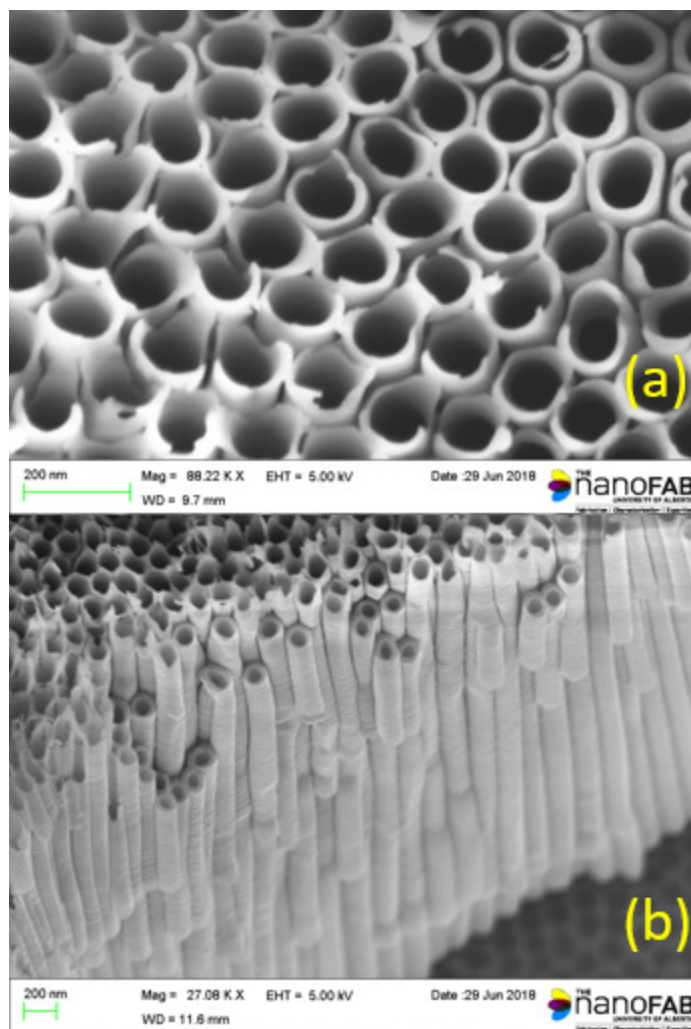
Figure 3. (a) Top-view FESEM image of TNTAs obtained by anodization of Ti foil in ethylene glycol containing 0.3 wt.% NH_4F and 4% DI at 60V for 2 hours and (b) Profile view FESEM image of the same TNTA sample showing the tubular cross-section of the nanotubes.

Figure 3 shows SEM images of a TNTA sample obtained by anodization of Ti foil. The nanotubes have diameters of *ca.* 100 nm and the as-prepared TNTAs are very hydrophilic [54, 62]. The roughness of the surfaces of the bare TNTA as well as the SAM-TNTA samples were also analyzed by using AFM. However, as presented in the AFM images of these samples in Supplementary Information Figure S1, the effect the SAM formation on surface roughness of the TNTA surface is obscured by the large roughness variation in the bare TNTA.

The freshly prepared TNTAs before functionalization with SAM are superhydrophilic, as indicated by the SCA determined from snapshot of the water droplet on bare TNTA shown in Figure 4. Figure 4 also shows the snapshots of the water droplets on TNTA functionalized with different SAMs. These images are fitted with the contact angle analysis software to determine the SCAs (θ_W and θ_{CB}) of the SAM-TNTAs as depicted in Scheme 1 and equation 1-4. Table 1 lists the alkyl phosphonic acids, the number of linearly linked carbons in the alkyl chain of the compounds, and the SCA values for the surfaces of the resulting SAM-TNTAs.

The plot of SCA versus number of linearly linked carbons in the SAM as depicted in Fig. 5a shows that an increase in the alkyl chain clearly results in increased SCA. Further analysis shows that the contact angle exhibits a sigmoidal growth curve (Figure 5a) with an initial rapid rise in the SCA with alkyl chain length below C_{10} followed by a plateau region with SCA < 150° (150° being considered the onset of superhydophobicity).
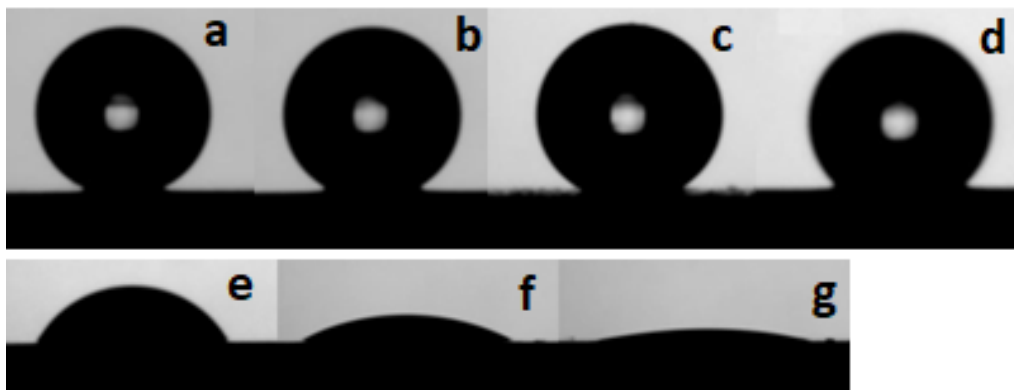

Figure 4. Snapshots of the water droplets on different SAM-TNTA surfaces: (a) PFDPA-TNTA, (b) ODPA-TNTA, (c) DPA-TNTA, (d) HPA-TNTA, (e) BPA-TNTA, (f) TBPA-TNTA, and (g) bare TNTA. The contact angles are listed in Table 1.

Table 1. Alkyl phosphonic acids, the number of linearly linked carbons in the alkyl chain of the compounds, and the contact angles of the surface of the SAM-TNTA. Contact angles are averaged from three different spots in the sample.

Chemical	Alkyl carbon chain length	Contact angle
1H,1H,2H,2H-Perfluorooctane phosphonic acid (PFDPA)	10	151.0 ± 4.0
n-Octadecyl phosphonic acid (ODPA)	18	147.7 ± 4.0
n-Decyl phosphonic acid (DPA)	10	144.7 ± 4.0
n-Hexyl phosphonic acid (HPA)	6	132.8 ± 13
n-Butyl phosphonic acid (BPA)	4	60.1 ± 10
tert-butyl phosphonic acid (TBPA)	2	23.8 ± 5.0
Bare TNTA	0	10.0±5.0

The terminal methyl or fluoromethyl groups in the alkylphosphonate monolayers are not wet by water. However, the achievement of extreme hydrophobicity is typically contingent on the formation of an ordered monolayer. When the alkyl chain is short in length, the Van der Waals interactions between adjacent molecules in the monolayer are weak due to which the monolayer is disordered (liquid-like) and there are a large number of defect sites where water molecules can bind to the surface. On the other hand, when the alkyl chain is long, the strong Van der Waals interactions between adjacent molecules promote the formation of a more ordered, semicrystalline monolayer with far fewer defect sites available for water molecules to bind to [63]. Eqn (4) for the Cassie-Baxter state can be re-written as:

$$f_s = \frac{1 + \cos\theta_{CB}}{1 + \cos\theta_c} \tag{5}$$

Eqn (5) shows that the term $\Theta = (1 + \cos\theta_{CB})$, is directly proportional to the contact area fraction parameter f_s, which is itself a measure of the number of high energy sites available for wetting by

water. Θ is itself also a direct measure of the free energy of the solid surface in the extended Fowkes theory [64]. The SAM-functionalized TNTA surface is assumed to consist of a limited number of distinct sites capable of binding water, which is the adsorbate in this case [65, 66]. In Figure 5b, the term Θ representing the number of binding sites, is plotted against the reciprocal of the number of carbon atoms in the alkyl chain of the molecules constituting the self-assembled monolayer (recognizing the inverse dependence of alkyl chain length on the number of binding sites explained above). We found the data was fit well by the Hill-Langmuir equation [67]:

$$\Theta = \frac{k[L]^n}{(K_{0.5})^n + [L]^n} \tag{6}$$

The fit parameters k and $K_{0.5}$ were extracted to be 2.08 and 0.228 respectively. The values of R^2 and red. χ^2, which express the goodness of the fit, were 0.99855 and 6.7×10^{-4} respectively. The extracted value of n, which was 3.53 strongly indicates the involvement of a cooperative mechanism [68] in the binding of water molecules to available defect sites wherein the binding of a single water molecule increases the likelihood of other water molecules binding to the same site.
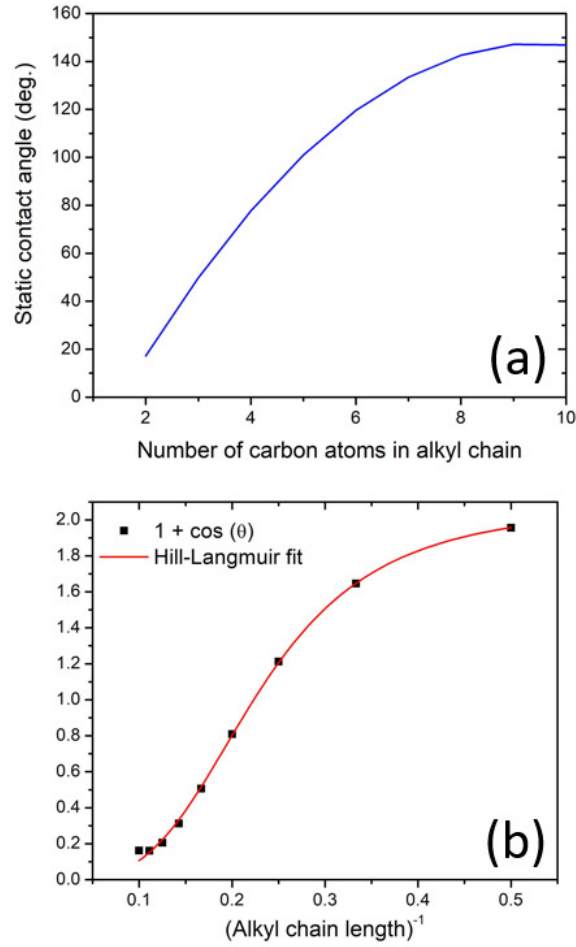
Figure 5. (a) Variation of the measured static contact angle (SCA) as a function of the number of carbon atoms in the alkyl chain backbone of the SAM-forming molecule and (b) Hill-Langmuir fit of a key Cassie-Baxter state parameter to the measured data.

The precipitation deposition of dissolved salts in water is the main source of sludge and scale formation on the walls of boilers and heat exchangers. This is because natural water has high concentrations of dissolved minerals composed of ions such as Na^+, Mg^{2+}, Ca^{2+}, K^+, Cl^-, SO_4^{2-}, HCO_3^-, CO_3^{2-} *etc* [69, 70]. Heating affects the solubility of salts and precipitation occurs upon supersaturation of the salts as water evaporates. In the case of salts with reverse solubility, precipitation occurs upon increasing the solution temperature, as is the case of scaling due to $CaCO_3$ [71]. Thus, to study how surface wettability affects fouling, the precipitation deposition of

sodium and magnesium salts on the SAM-TNTA surfaces was examined and compared with that of the unmodified TNTA substrate. SCA measurements showed that the pure water and salt solutions (0.1 M NaCl and 0.1 M MgCl$_2$) used in this study exhibited comparable SCA values on each surface. As shown in Figure 6a, only about half of each 1 cm x 4cm Ti foil is anodized to form TNTA (light yellowish-brown color portion of each sample), while the other half of the sample is pristine Ti with a native oxide layer. It is expected that these samples are entirely covered by a monolayer of SAM since the samples were completely immersed in the alkyl phosphonic acid solution during the functionalization process. However, the wettability or SCA of the SAM modified Ti native oxide (SAM-TNO) is known to be substantially less than the SAM-TNTA region [56].
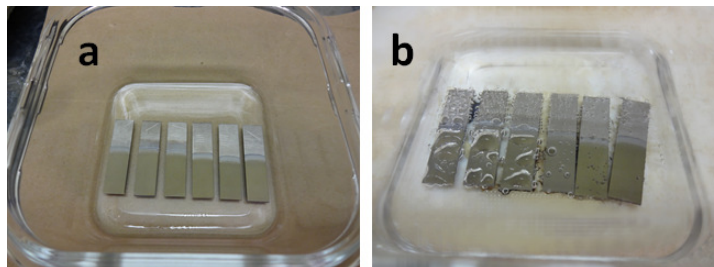

Figure 6. (a) As prepared SAM-TNTAs before precipitation deposition of salts on their surfaces. Only the lower half of each sample has TNTA (light yellowish-brown color) whereas the upper half is Ti with native oxide layer. The samples from left to right are modified with SAM of PFDPA, ODPA, DPA, HPA, BPA, and TBPA, arranged in order of increasing wettability, and (b) The same samples at a temperature near the boiling point of the aqueous solution containing 0.1 M NaCl and 0.1 M MgCl$_2$. The three leftmost samples, all possessing a SCA > 145° showed enhanced bubble formation.

Upon heating the samples immersed in an aqueous solution containing 0.1 M NaCl and 0.1 M MagCl$_2$, a clear distinction is visible based on how the water evaporates on SAM-TNTA surfaces with SCA > 144° compared to SAM-TNTA surfaces with SCA ≤ 134° as shown in Figure 6b.

Samples with SCA ≥ 144º form Cassie-Baxter states that facilitate the nucleation of bubbles leading to the formation of a sheet of air saturated water vapor beneath the saline solution, thereby impeding the interaction between the SAM-TNTA surface and the saline solution above. This observation is supported by previous studies that prove nanobubbles are present at the interface of water and the hydrophobic surface [72-75]. Furthermore, the hydrophobic surface has a high affinity for air, and nanobubbles are believed to be responsible for the relatively long range hydrophobic behavior (hundreds of nanometers) [76-80]. Another notable observation is the formation of intense blue color in samples with SCA ≤ 134º (most clearly seen in Figure 7a). It should be noted that this color is not due to an interference effect because the color is unaffected by viewing angle and it fades away after several heating cycles as observed in Figures. 7a-f. Instead, it is caused by the surface intercalation of cations from salt in the aqueous solution into TiO_2. Thus, a high concentration of Ti^{3+} states on the sub-surface below the SAM layer becomes present, leading to an intense blue color which is well-established in the scientific literature [81]. The very fact that such a blue color does not develop for SAM-TNTA surfaces with SCA > 134º is the first major piece of evidence showing that a high degree of hydrophobicity impedes the interaction of dissolved ions in water with the TiO_2 sub-surface in SAM-TNTA samples.
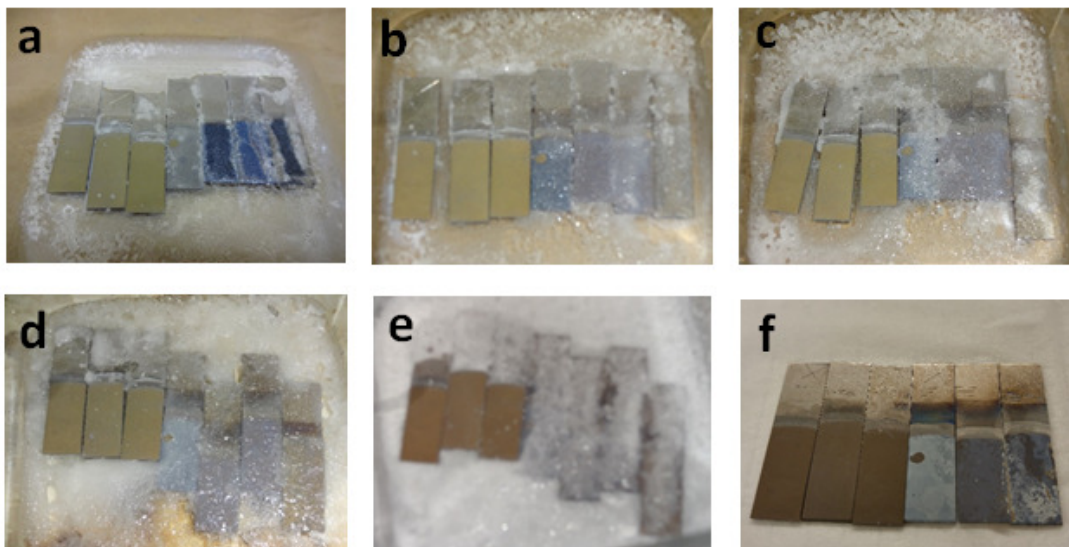
Figure 7. Six SAM-TNTA samples (from left to right, using PFDPA-TNTA, ODPA-TNTA, DPA-TNTA, HPA-TNTA, BPA-TNTA,TBPA-TNTA, and bare TNTA with SCA of 151, 148, 145, 133, 60, 24, 10° respectively) and an unmodified bare TNTA sample on the farthest right, taken at the end of successive evaporation of 100 ml of saline (0.1 M NaCl and 0.1 M MgCl$_2$) solution in a square (10cm x 10cm) glass vial. The pictures from left to right (a) 1st, (b) 2nd, (c) 3rd, (d) 4th, and (e) 5th were recorded after evaporation of water and deposition of the salts on the SAM-TNTA surfaces (See Figure 8). As the samples were not washed at the end of each step, increasing deposition of the salts on the SAM-TNTA surfaces is evident with successive evaporation; (f) shows the six SAM-TNTA samples recorded after washing out the deposited salts at the end of the experiment.

Figure 7 shows several pictures taken at the end of the subsequent evaporation cycles of a saline solution (for each cycle, 100 ml of 0.1 M NaCl and 0.1 M MagCl$_2$ was deposited and evaporated). The deposition of the salts is clearly visible on the surface of the glass vial, on the SAM-TNTA surfaces of samples with a SCA $\leq$ 134°, and on the surface of the hydrophilic bare Ti sample (farthest right in Fig. 7a-e). It is worth noting in Figure 7 that samples with SCA $\leq$ 134° have scale deposition similar to that on the highly hydrophilic unmodified TNTA sample. Figure 7 also shows that for the SAM-TNTA samples with SCA > 144°, no visible salt deposit can be observed on their surfaces. This observation is supported by characterization of the surfaces of

these samples using energy-dispersive X-ray spectroscopy (EDX) which shows the elements constituting the salts (Na, Mg, Cl) are present at levels close to the detection limit (< 0.3 wt.%) of EDX (see below). However, even in these samples, salt deposits are visible on the bare SAM-TNO portion of the samples. The improved performance of SAM-TNTA versus SAM-TNO is attributed the formation of nanobubbles on the SAM-TNTA hydrophobic surface and the trapped air in the associated Cassie-Baxter states. The subsequent formation of a thin sheet of air saturated water vapor as displayed in Figure 6b thus efficiently impeded the deposition of salt scale on these surfaces. Successive evaporation cycles of saline salt, without washing out the salts deposited in the previous evaporation, led to deposition of thicker and thicker layers of salt scale on the surfaces of the SAM-TNTAs with SCA $\leq 134^\circ$. This does not occur due to layer-by-layer deposition as both NaCl and MaCl$_2$ are highly soluble in water (6.1 M and 3.8 M respectively) and their solubilities increase with temperature. Instead, fresh salt deposits are formed on the surfaces upon each evaporation step on these SAM-TNTAs ~~with SCA ≤ 134°~~, and the increased thickness of the salt layer occurs because the effective concentration of salt in the saline increases each cycle (up to 0.5 M of NaCl and 0.5 MgCl$_2$ during the fifth cycle). It is remarkable that the SAM-TNTAs are able to resist scale buildup even at these higher concentrations.

To further confirm that there is no significant deposition of salts on the surfaces of the three SAM-TNTAs with SCA $\geq 144^\circ$, their surfaces at the end of the 5th deposition cycle (Figure 7e) were examined by EDX. Figure 8 presents the EDX spectra and SEM images before washing the samples after the 5th evaporation-deposition cycle. The EDX spectra showed the presence of Ti, O, C, F, and P with minute amounts of elements Cl, Na and no detectable Mg. Since these samples (SAM-TNTAs) are composed of titanium dioxide functionalized with a monolayer of alkyl phosphonate, the presence of Ti and O, and a small amount of C and P is expected. The significant

amount of F (> 5 wt.%) in all samples likely originated due to the fluoride-containing electrolyte used during anodization.
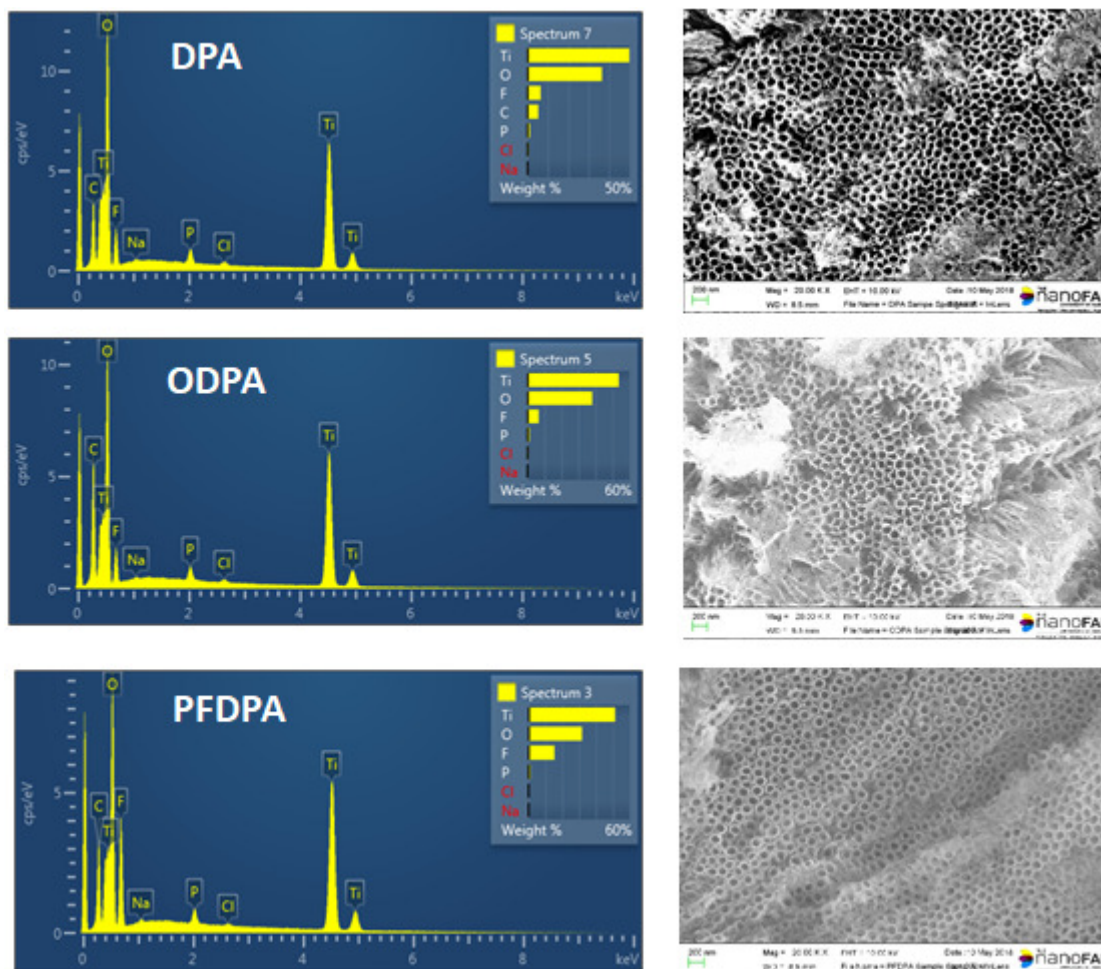

Figure 8. EDX spectra before washing of samples with (CA ≥ 145º) recorded after the 5th evaporation-deposition cycle and the corresponding SEM images showing the SAM-TNTA, as well as small patches of debris that sometimes form during anodization.

EDX analysis showed that among the elements making up the salts used in the fouling experiments, Cl has the highest contribution, constituting as high as 0.4 wt % of the surface elements, followed by Na with 0.2 % and no detectable Mg. The exact amount of Cl and Na varied from spot to spot on the sample and in some spots they were not detectable. Furthermore, it is not unreasonable to believe that a significant amount of Cl and Na detected on the surface of these samples may have

originated as a contaminant from chemicals used in the preparation of SAM and anodization. These results clearly indicate that surfaces with threshold hydrophobicity (SCA $\geq$ 145°) can inhibit precipitation fouling of the surface.

A pertinent question is how the surface wettability endured the five successive evaporation induced fouling cycles particularly for samples which appear to inhibit fouling. To answer, we have measured the SCA before and after a final rinse with water following the five fouling cycles. Remarkably, the SCAs of PFDPA-TNTA, ODPA-TNTA and DPA-TNTA measured before rinsing were 155.6°, 151.1° and 149.3° respectively, indicating that their water repelling property increased after the 5 heating cycles in saline water (as compared with their SCAs before fouling experiment listed in Table 1). In addition, rinsing of the sample had no effect on their SCAs (154.2°, 151.9° and 150.3° respectively for PFDPA-TNTA, ODPA-TNTA and DPA-TNTA). These results indicate that both the nanostructure and SAM layer are not only intact but their SCAs have increased. The increase in the observed SCAs may be due to the thermally induced increased crystallinity of the SAM layers of these samples. In contrast, the other three samples (with initial SCA $\leq$ 134°) became highly hydrophilic or superhydrophilic (with an SCA close to zero after washing off the deposited salts). Comparison of the images of these 3 samples before (Figure 6a) and after (Figure 7f), show degradation due to fouling due after repeated salt deposition-dissolution cycles, as indicated by both the change in the color and the texture.

To further characterize the stability of the SAM layer in the SAM-TNTA samples against five successive heating-evaporation-precipitation deposition cycles in aqueous saline solution, the DRIFTS spectra of the samples were recorded after washing off the deposited salts. The spectra of PFDPA-TNTA, ODPA-TNTA and DPA-TNTA were unaffected by the treatment. However, the HPA-TNTA, BPA-TNTA and TBPA-TNTA samples did not show the presence of the signature

alkyl band, including the band in the C-H stretching region. This suggests that the SAM layers were probably destroyed by the fouling experiment.

4. Conclusion

The relationship between fouling determined by precipitation deposition of water soluble salts and wettability of the surface has been investigated for SAM functionalized titanium dioxide nanotube array on titanium foil (SAM-TNTAs). The wettability of the surface, determined by the SCA of the SAM-TNTA, was tuned using the alkyl chain length of the SAM used to functionalize the TNTA. The dependence of the SCA on the alkyl chain length followed a sigmoidal growth curve, and an excellent fit to the experimental data was obtained using the Hill-Langmuir equation. The SAM-TNTA surfaces with wettability above the threshold hydrophobicity (~ 144 °) were observed to inhibit the precipitation deposition of water soluble salts on their surfaces. The onset of the distinct anti-fouling surface property observed in SAM-TNTA samples with SCA of 144° or higher is remarkable, and we believe that there is considerable room for further study. We attribute the antifouling property of the SAM-TNTAs to the presence of nanobubbles in the interface of water-hydrophobic surface and high affinity of air to hydrophobic surface, thus forming of a thin sheet of water saturated air at the water-solid interface. However, an even deeper understanding of the physical processes that allow the SAM-TNTAs to exhibit superior fouling resistance could allow for the strategies employed in this study to be expanded to other material and morphological systems.

References

[1] K. Thulukkanam, Heat exchanger design handbook, CRC Press, 2013.

[2] K. Thulukkanam, Heat exchanger design handbook, CRC Press, 2000.

[3] A. Pritchard, The economics of fouling, in: Fouling Science and Technology, Springer, 1988, pp. 31-45.

[4] X. Zhao, X.D. Chen, A critical review of basic crystallography to salt crystallization fouling in heat exchangers, Heat Transfer Eng., 34 (2013) 719-732.

[5] O. Ajayi, S. Ogbonnaya, Fouling Phenomenon and its Effect on Heat Exchanger: A Review, Frontiers in Heat and Mass Transfer (FHMT), 9 (2017).

[6] A. Karimi, D. Karig, A. Kumar, A.M. Ardekani, Interplay of physical mechanisms and biofilm processes: review of microfluidic methods, Lab Chip, 15 (2015) 23-42.

[7] A. Kumar, D. Karig, R. Acharya, S. Neethirajan, P.P. Mukherjee, S. Retterer, M.J. Doktycz, Microscale confinement features can affect biofilm formation, Microfluidics and Nanofluidics, 14 (2013) 895-902.

[8] X. Liu, L. Jungang, Z. Qianya, F. Jinlai, L. Yingli, S. Jingxin, The analysis and prediction of scale accumulation for water-injection pipelines in the Daqing Oilfield, Journal of Petroleum Science and Engineering, 66 (2009) 161-164.

[9] R.L. Townsin, The Ship Hull Fouling Penalty, Biofouling, 19 (2003) 9-15.

[10] D. Oliveira, A.I. Larsson, L. Granhag, Effect of ship hull form on the resistance penalty from biofouling, Biofouling, 34 (2018) 262-272.

[11] Z. Xu, S. Yang, S. Guo, H. Zhao, B. Qi, Z. Zhang, Costs due to utility boiler fouling in China, Heat Transfer—Asian Research, 34 (2005) 53-63.

[12] G. Azimi, Y. Cui, A. Sabanska, K.K. Varanasi, Scale-resistant surfaces: Fundamental studies of the effect of surface energy on reducing scale formation, Appl. Surf. Sci., 313 (2014) 591-599.

[13] A.J. Meuler, J.D. Smith, K.K. Varanasi, J.M. Mabry, G.H. McKinley, R.E. Cohen, Relationships between water wettability and ice adhesion, ACS Appl. Mater. Inter., 2 (2010) 3100-3110.

[14] M. Liu, S. Wang, L. Jiang, Nature-inspired superwettability systems, Nat. Rev. Mater., 2 (2017) 17036.

[15] S. Zhang, J. Huang, Z. Chen, Y. Lai, Bioinspired special wettability surfaces: from fundamental research to water harvesting applications, Small, 13 (2017).

[16] G. Bracco, B. Holst, Surface science techniques, Springer Science & Business Media, 2013.

[17] T. Chau, W. Bruckard, P. Koh, A. Nguyen, A review of factors that affect contact angle and implications for flotation practice, Adv. Colloid Interface Sci., 150 (2009) 106-115.

[18] G. Kumar, K.N. Prabhu, Review of non-reactive and reactive wetting of liquids on surfaces, Adv. Colloid Interface Sci., 133 (2007) 61-89.

[19] D. Quéré, Wetting and roughness, Annu. Rev. Mater. Res., 38 (2008) 71-99.

[20] C.R. Crick, I.P. Parkin, Preparation and Characterisation of Super-Hydrophobic Surfaces, Chemistry-A European Journal, 16 (2010) 3568-3588.

[21] L. Wen, Y. Tian, L. Jiang, Bioinspired super-wettability from fundamental research to practical applications, Angew. Chem., Int. Ed., 54 (2015) 3387-3399.

[22] D. Li, A. Neumann, Contact angles on hydrophobic solid surfaces and their interpretation, J. Colloid Interface Sci., 148 (1992) 190-200.

[23] A. Marmur, Solid-surface characterization by wetting, Annu. Rev. Mater. Res., 39 (2009) 473-489.

[24] T. Young, III. An essay on the cohesion of fluids, Philosophical transactions of the royal society of London, 95 (1805) 65-87.

[25] R.N. Wenzel, Resistance of solid surfaces to wetting by water, Industrial & Engineering Chemistry, 28 (1936) 988-994.

[26] A. Cassie, S. Baxter, Wettability of porous surfaces, Transactions of the Faraday society, 40 (1944) 546-551.

[27] J.P. Folkers, C.B. Gorman, P.E. Laibinis, S. Buchholz, G.M. Whitesides, R.G. Nuzzo, Self-Assembled Monolayers of Long-Chain Hydroxamic Acids on the Native Oxides of Metals

Langmuir, 11 (1995) 813-824.

[28] C. Yee, G. Kataby, A. Ulman, T. Prozorov, H. White, A. King, M. Rafailovich, J. Sokolov, A. Gedanken, Self-assembled monolayers of alkanesulfonic and -phosphonic acids on amorphous iron oxide nanoparticles, Langmuir, 15 (1999) 7111-7115.

[29] A. Badia, R.B. Lennox, L. Reven, A dynamic view of self-assembled monolayers, Acc. Chem. Res., 33 (2000) 475-481.

[30] J.C. Love, L.A. Estroff, J.K. Kriebel, R.G. Nuzzo, G.M. Whitesides, Self-assembled monolayers of thiolates on metals as a form of nanotechnology, Chem. Rev., 105 (2005) 1103-1169.

[31] S. Onclin, B.J. Ravoo, D.N. Reinhoudt, Engineering silicon oxide surfaces using self-assembled monolayers, Angew. Chem.-Int. Edit., 44 (2005) 6282-6304.

[32] B.M. Silverman, K.A. Wieghaus, J. Schwartz, Comparative properties of siloxane vs phosphonate monolayers on a key titanium alloy, Langmuir, 21 (2005) 225-228.

[33] D.K. Aswal, S. Lenfant, D. Guerin, J.V. Yakhmi, D. Vuillaume, Self assembled monolayers on silicon for molecular electronics, Anal. Chim. Acta, 568 (2006) 84-108.

[34] T. Darmanin, F. Guittard, Wettability of conducting polymers: from superhydrophilicity to superoleophobicity, Prog. Polym. Sci., 39 (2014) 656-682.

[35] J. Li, S. Ji, G. Zhang, H. Guo, Surface-modification of poly (dimethylsiloxane) membrane with self-assembled monolayers for alcohol permselective pervaporation, Langmuir, 29 (2013) 8093-8102.

[36] E. Decker, S. Garoff, Contact line structure and dynamics on surfaces with contact angle hysteresis, Langmuir, 13 (1997) 6321-6332.

[37] A.M. Almanza-Workman, S. Raghavan, S. Petrovic, B. Gogoi, P. Deymier, D.J. Monk, R. Roop, Characterization of highly hydrophobic coatings deposited onto pre-oxidized silicon from water dispersible organosilanes, Thin Solid Films, 423 (2003) 77-87.

[38] T. Otitoju, A. Ahmad, B. Ooi, Superhydrophilic (superwetting) surfaces: A review on fabrication and application, Journal of industrial and engineering chemistry, 47 (2017) 19-40.

[39] F.C. Birjandi, J. Sargolzaei, Super-non-wettable surfaces: a review, Colloids and Surfaces A: Physicochemical and Engineering Aspects, 448 (2014) 93-106.

[40] A.M. Mohamed, A.M. Abdullah, N.A. Younan, Corrosion behavior of superhydrophobic surfaces: A review, Arabian journal of chemistry, 8 (2015) 749-765.

[41] L. Zhang, N. Zhao, J. Xu, Fabrication and application of superhydrophilic surfaces: a review, J. Adhes. Sci. Technol., 28 (2014) 769-790.

[42] A. Marmur, Super-hydrophobicity fundamentals: implications to biofouling prevention, Biofouling, 22 (2006) 107-115.

[43] E. Vazirinasab, R. Jafari, G. Momen, Application of superhydrophobic coatings as a corrosion barrier: A review, Surf. Coat. Technol., (2017).

[44] P. Zhang, F. Lv, A review of the recent advances in superhydrophobic surfaces and the emerging energy-related applications, Energy, 82 (2015) 1068-1087.

[45] L. Cao, A.K. Jones, V.K. Sikka, J. Wu, D. Gao, Anti-icing superhydrophobic coatings, Langmuir, 25 (2009) 12444-12448.

[46] M. Nosonovsky, B. Bhushan, Superhydrophobic surfaces and emerging applications: non-adhesion, energy, green engineering, Curr. Opin. Colloid Interface Sci., 14 (2009) 270-280.

[47] Q. Wen, Z. Guo, Recent advances in the fabrication of superhydrophobic surfaces, Chem. Lett., 45 (2016) 1134-1149.

[48] W. Jiang, J. He, F. Xiao, S. Yuan, H. Lu, B. Liang, Preparation and antiscaling application of superhydrophobic anodized CuO nanowire surfaces, Ind. Eng. Chem. Res., 54 (2015) 6874-6883.

[49] A.B. Tesler, P. Kim, S. Kolle, C. Howell, O. Ahanotu, J. Aizenberg, Extremely durable biofouling-resistant metallic surfaces based on electrodeposited nanoporous tungstite films on steel, Nat. Commun., 6 (2015) 8649.

[50] H. Li, S. Yu, X. Han, Y. Zhao, A stable hierarchical superhydrophobic coating on pipeline steel surface with self-cleaning, anticorrosion, and anti-scaling properties, Colloids and Surfaces A: Physicochemical and Engineering Aspects, 503 (2016) 43-52.

[51] C.-W. Yao, D. Sebastian, I. Lian, Ö. Günaydın-Şen, R. Clarke, K. Clayton, C.-Y. Chen, K. Kharel, Y. Chen, Q. Li, Corrosion Resistance and Durability of Superhydrophobic Copper Surface in Corrosive NaCl Aqueous Solution, Coatings, 8 (2018) 70.

[52] T. Shokuhfar, A. Hamlekhan, J.-Y. Chang, C.K. Choi, C. Sukotjo, C. Friedrich, Biophysical evaluation of cells on nanotubular surfaces: the effects of atomic ordering and chemistry, International Journal of Nanomedicine, 9 (2014) 3737-3748.

[53] Y. Zhao, Q. Xing, J. Janjanam, K. He, F. Long, K.-B. Low, A. Tiwari, F. Zhao, R. Shahbazian-Yassar, C. Friedrich, T. Shokuhfar, Facile electrochemical synthesis of antimicrobial TiO(2) nanotube arrays, International Journal of Nanomedicine, 9 (2014) 5177-5187.

[54] D.H. Shin, T. Shokuhfar, C.K. Choi, S.-H. Lee, C. Friedrich, Wettability changes of TiO 2 nanotube surfaces, Nanotechnology, 22 (2011) 315704.

[55] S. Farsinezhad, P. Waghmare, B.D. Wiltshire, S. Amiri, S.K. Mitra, K. Shankar, The Wetting Behavior of TiO2 Nanotube Arrays With Perfluorinated Surface Functionalization, in: ASME 2014 International Mechanical Engineering Congress and Exposition, American Society of Mechanical Engineers, 2014, pp. V009T012A071-V009T012A071.

[56] S. Farsinezhad, P.R. Waghmare, B.D. Wiltshire, H. Sharma, S. Amiri, S.K. Mitra, K. Shankar, Amphiphobic surfaces from functionalized TiO 2 nanotube arrays, RSC Adv., 4 (2014) 33587-33598.

[57] P. Kar, A. Pandey, J.J. Greer, K. Shankar, Ultrahigh sensitivity assays for human cardiac troponin I using TiO 2 nanotube arrays, Lab Chip, 12 (2012) 821-828.

[58] A. Mohammadpour, B. Wiltshire, Y. Zhang, S. Farsinezhad, A. Askar, R. Kisslinger, Y. Ren, P. Kar, K. Shankar, 100-fold improvement in carrier drift mobilities in alkanephosphonate-passivated monocrystalline TiO2 nanowire arrays, Nanotechnology, 28 (2017) 144001.

[59] M.H. Zarifi, S. Farsinezhad, B.D. Wiltshire, M. Abdorrazaghi, N. Mahdi, P. Kar, M. Daneshmand, K. Shankar, Effect of phosphonate monolayer adsorbate on the microwave photoresponse of TiO2 nanotube membranes mounted on a planar double ring resonator, Nanotechnology, 27 (2016) 375201.

[60] P. Roy, R. Kisslinger, S. Farsinezhad, N. Mahdi, A. Bhatnagar, A. Hosseini, L. Bu, W. Hua, B.D. Wiltshire, A. Eisenhawer, P. Kar, K. Shankar, All-solution processed, scalable superhydrophobic coatings on stainless steel surfaces based on functionalized discrete titania nanotubes, Chem. Eng. J. (Lausanne), 351 (2018) 482-489.

[61] W. Hua, P. Kar, P. Roy, L. Bu, L. Shoute, P. Kumar, K. Shankar, Resistance of Superhydrophobic Surface-Functionalized TiO2 Nanotubes to Corrosion and Intense Cavitation, Nanomaterials, 8 (2018) 783.

[62] S. Sorcar, A. Razzaq, H. Tian, C.A. Grimes, S.-I. In, Facile electrochemical synthesis of anatase nano-architectured titanium dioxide films with reversible superhydrophilic behavior, Journal of Industrial and Engineering Chemistry, 46 (2017) 203-211.

[63] E.S. Gawalt, M.J. Avaltroni, N. Koch, J. Schwartz, Self-Assembly and Bonding of Alkanephosphonic Acids on the Native Oxide Surface of Titanium, Langmuir, 17 (2001) 5736-5738.

[64] D.Y. Kwok, D. Li, A.W. Neumann, Fowkes' surface tension component approach revisited, Colloids and Surfaces A: Physicochemical and Engineering Aspects, 89 (1994) 181-191.

[65] I. Langmuir, The constitution and fundamental properties of solids and liquids. Part I. Solids, J. Am. Chem. Soc., 38 (1916) 2221-2295.

[66] A.V. Hill, The possible effects of the aggregation of the molecules of haemoglobin on its dissociation curves, J. Physiol., 40 (1910) 4-7.

[67] R. Gesztelyi, J. Zsuga, A. Kemeny-Beke, B. Varga, B. Juhasz, A. Tosaki, The Hill equation and the origin of quantitative pharmacology, Archive for History of Exact Sciences, 66 (2012) 427-438.

[68] M.I. Stefan, N. Le Novère, Cooperative Binding, PLoS Comput. Biol., 9 (2013) e1003106.

[69] J.I. Drever, G. Marion, The geochemistry of natural waters: surface and groundwater environments, J. Environ. Qual., 27 (1998) 245-245.

[70] J.D. Hem, Study and interpretation of the chemical characteristics of natural water, Department of the Interior, US Geological Survey, 1985.

[71] N. Yanagisawa, Case study of calcium carbonate scale at EGS and hot spring binary system, in: Proceedings World Geothermal Congress, 2015.

[72] Y.W. Liu, X.R. Zhang, A unified mechanism for the stability of surface nanobubbles: Contact line pinning and supersaturation, J. Chem. Phys., 141 (2014).

[73] Y.W. Liu, X.R. Zhang, Molecular dynamics simulation of nanobubble nucleation on rough surfaces, J. Chem. Phys., 146 (2017).

[74] X. Sheng, Z. Liu, R.S. Zeng, L.P. Chen, X.J. Feng, L. Jiang, Enhanced Photocatalytic Reaction at Air-Liquid-Solid Joint Interfaces, J. Am. Chem. Soc., 139 (2017) 12402-12405.

[75] Z.Q. Song, C.L. Xu, X. Sheng, X.J. Feng, L. Jiang, Utilization of Peroxide Reduction Reaction at Air-Liquid-Solid Joint Interfaces for Reliable Sensing System Construction, Adv. Mater., 30 (2018).

[76] Y. Xing, X. Gui, L. Pan, B.-E. Pinchasik, Y. Cao, J. Liu, M. Kappl, H.-J. Butt, Recent experimental advances for understanding bubble-particle attachment in flotation, Adv. Colloid Interface Sci., 246 (2017) 105-132.

[77] C. Shi, X. Cui, X. Zhang, P. Tchoukov, Q. Liu, N. Encinas, M. Paven, F. Geyer, D. Vollmer, Z. Xu, Interaction between air bubbles and superhydrophobic surfaces in aqueous solutions, Langmuir, 31 (2015) 7317-7327.

[78] I.U. Vakarelski, D.Y. Chan, J.O. Marston, S.T. Thoroddsen, Dynamic air layer on textured superhydrophobic surfaces, Langmuir, 29 (2013) 11074-11081.

[79] M. Krasowska, J. Zawala, K. Malysa, Air at hydrophobic surfaces and kinetics of three phase contact formation, Adv. Colloid Interface Sci., 147 (2009) 155-169.

[80] R. Colaço, A. Serro, B. Saramago, On the stability of bubbles trapped at a solid–liquid interface: a thermodynamical approach, Surf. Sci., 603 (2009) 2870-2873.

[81] S. Södergren, H. Siegbahn, H. Rensmo, H. Lindström, A. Hagfeldt, S.-E. Lindquist, Lithium Intercalation in Nanoporous Anatase TiO2 Studied with XPS, J. Phys. Chem. B, 101 (1997) 3087-3090.